ACS OMEGA

http://pubs.acs.org/journal/acsodf

Article

Biocompatible Aza-BODIPY-Biotin Conjugates for Photodynamic Therapy of Cancer

Dhiraj Dutta,[¶] Rajshree R. Nair,[¶] Sreejith Mangalath, S. Asha Nair,* Joshy Joseph, Pranjal Gogoi,* and Danaboyina Ramaiah

Cite This: *ACS Omega* 2023, 8, 26180−26190

Read Online

ACCESS | Metrics & More | Article Recommendations | Supporting Information

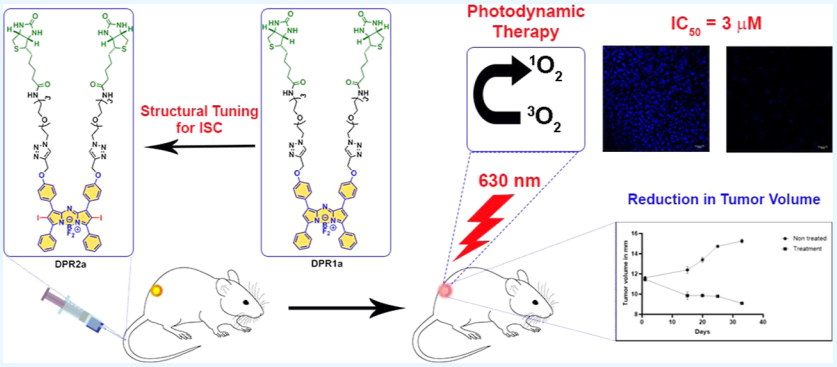

ABSTRACT: With an objective to develop efficient photosensitizers to cancerous tissues, we synthesized two novel biocompatible sensitizers based on aza-BODIPYs incorporated with heavy atoms and biotin moieties. The bioconjugates **DPR2a** and **DPR2b** exhibited a favorable absorption range (600−750 nm) with excellent triplet-state quantum yields (up to 79%) and singlet oxygen generation yields (up to 75%). In vitro photobiological investigations employing MDA-MB-231 breast cancer cell lines exhibited rapid cellular uptake, negligible dark toxicity, and high photocytotoxicity. The mechanism of cell death of these systems was predominantly due to the mitochondrial damage, leading to apoptosis mediated *via* the generation of singlet oxygen-triggered reactive oxygen species. The in vivo studies with the representative conjugate **DPR2a** employing female NOD/SCID mice models showed inhibition in tumor growth and significantly decreased tumor volume post photodynamic therapy (PDT) treatment. Our results validate that both **DPR2a** and **DPR2b** with iodine incorporation exhibit favorable and superior photophysical and photobiological aspects and demonstrate thereby their potential applications in imaging and PDT of cancer.

1. INTRODUCTION

Photodynamic therapy (PDT) has been an evolving area in cancer research and represents a favorable and effective approach over conventional therapies.[1] In PDT, a photosensitizer (PS) plays an important role by releasing cytotoxic reactive oxygen species (ROS).[2−4] To get a robust and versatile PS, various PSs such as porphyrins, rose-bengal, porphycenes, phthalocyanines, methylene blue, chlorins, squaraines, bacteriochlorins, BODIPY, aza-BODIPY, and their analogues have been developed.[5−8] For the effective PDT outcome, the intrinsic efficacy of the PS is one of the significant components. The search for an ideal sensitizer is highly focused; as a result, third-generation PSs were developed from second-generation PSs by conjugating with specific moieties for targeted delivery. Various amino acids,[9] peptides,[10,11] carbohydrates,[12] and antibodies[13] or by encapsulation into carriers like liposomes,[14] micelles,[15−17] and polymeric nanoparticles have been used for conjugation.[15,18,19] However, in most of the cases, appended modifications are required, which reduce the specificity, toxicity, and shelf life of the PSs. In the last few decades, biotin has attracted tremendous importance among the scientific and pharmaceutical communities and has been used as a small target-specific moiety for cancer cells, drug monitoring, and therapy due to its low molecular weight, high tumor specificity, and most importantly biocompatibility.[20] Nevertheless, a few PSs like phthalocyanine,[15,21−23] porphyrin,[24] chlorins,[25,26] nile blue,[27] ruthenium metal complexes,[28,29] and iron(III) metal complexes[30] have been conjugated with biotin for targeted PDT. Biotin has also been conjugated with aza-BODIPYs; however, this was limited particularly for drug monitoring and bioimaging studies.[31]

Received: April 10, 2023
Accepted: May 30, 2023
Published: June 21, 2023

Scheme 1. Synthesis of Aza-BODIPYs: 1d, 1e, and 2d, 2e

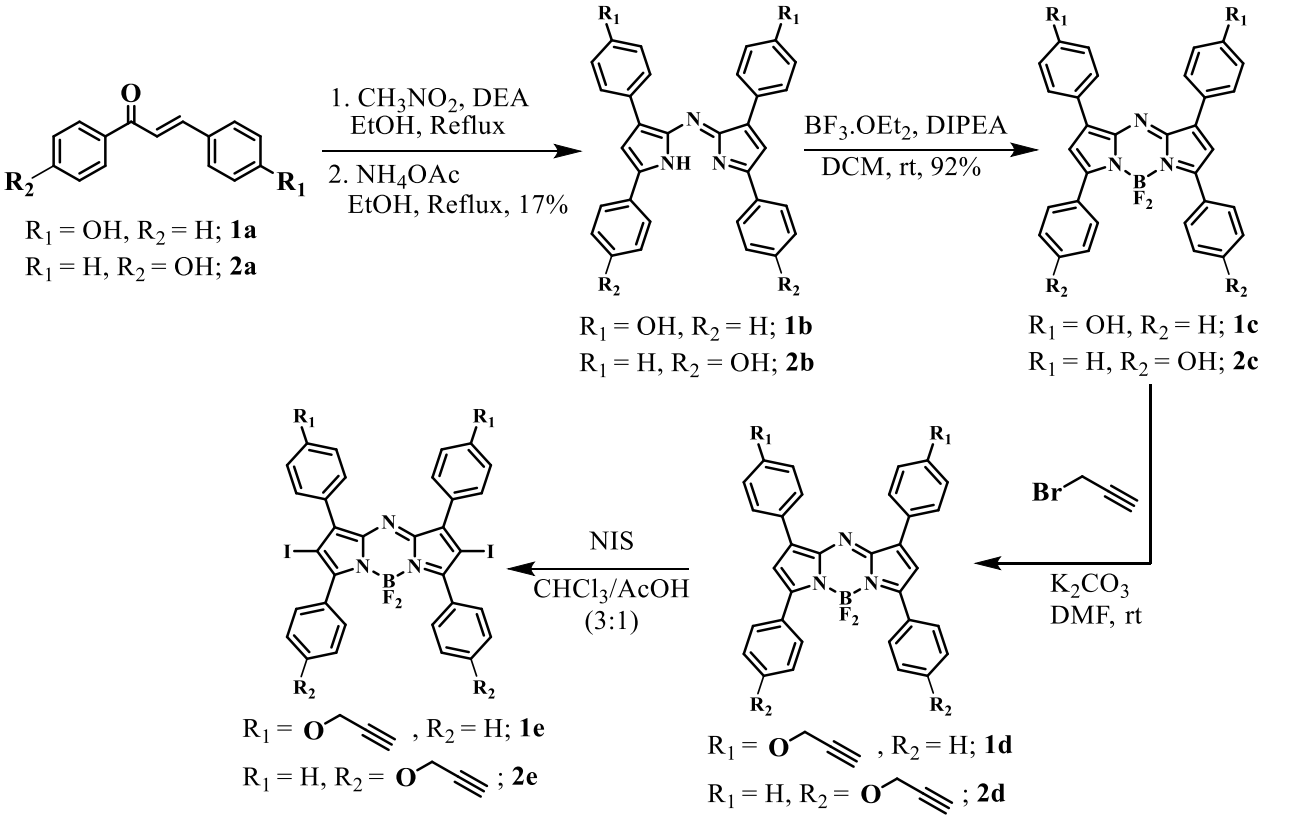

Scheme 2. Synthesis of AzBiotin from PEG_3 and Biotin

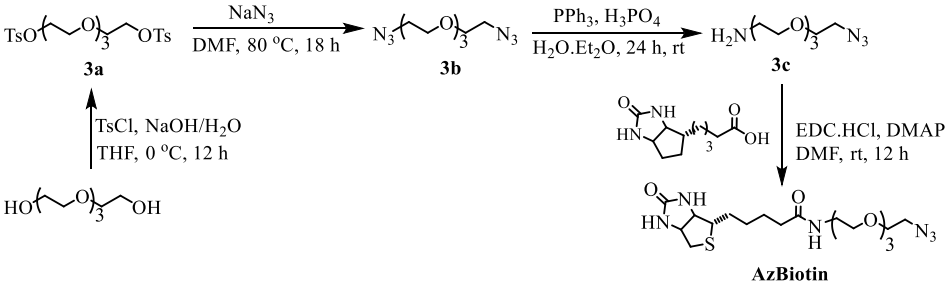

Recently, aza-BODIPYs have attracted considerable interest in bioapplications due to their ease of synthesis, flexible framework, high molar attenuation coefficient, tunable photophysical parameters, and remarkable photostability.[17,19,31−38] Although the photophysical and photobiological properties of these classes of dyes have been investigated, studies pertaining to clinical applications are rather limited.[19,31] Recently, aza-BODIPYs have been formulated as self-assembled micelles with aspartic acid[39] and conjugated with glucose[40] and amino acid[9] to enhance its PDT efficacy.

Herein, to overcome the shortcomings of third-generation PSs, we designed two novel aza-BODIPY-biotin conjugates **DPR2a** and **DPR2b** having two biotin units for PDT of cancer. The framework of the PSs consists of three parts: aza-BODIPY, PEG-3, and biotin (Schemes 1−3). Initially, the non-iodinated aza-BODIPY-biotin conjugates **DPR1a** and **DPR1b** were synthesized (Scheme 3). They showed good fluorescence properties but lacked significant transient absorption for the triplet state which was vital for PDT. So, we planned to incorporate heavy atoms to the core of aza-BODIPYs for the triplet-state transition through the heavy atom effect,[33] and accordingly, we synthesized our targeted conjugates **DPR2a** and **DPR2b** (Schemes 1 and 3). Both the aza-BODIPYs **DPR2a** and **DPR2b** exhibited good absorption in the photobiological window with excellent extinction coefficient, good triplet-state quantum yields, and singlet oxygen generation quantum yields. Also, these systems exhibited efficient photodynamic activity in biotin receptor-positive triple-negative MDA-MB-231 breast cancer cells in vitro and were effective in hindering the tumor growth in the in vivo female NOD/SCID mice models, demonstrating thereby their effectiveness as a sensitizer for PDT applications.

2. RESULTS AND DISCUSSION

2.1. Synthesis and Photophysical Studies. Our experiments for the synthesis of compounds **1d** and **2d** started with 4-hydroxychalcone **1a** and 4′-hydroxychalcone **2a** as starting materials following a reported procedure (Scheme 1).[41] The targeted aza-BODIPY-biotin conjugates **DPR1a** and **DPR1b** were synthesized by performing click reaction of compounds

https://doi.org/10.1021/acsomega.3c02416
ACS Omega 2023, 8, 26180−26190

Scheme 3. Synthesis of Aza-BODIPY-Biotin Conjugates

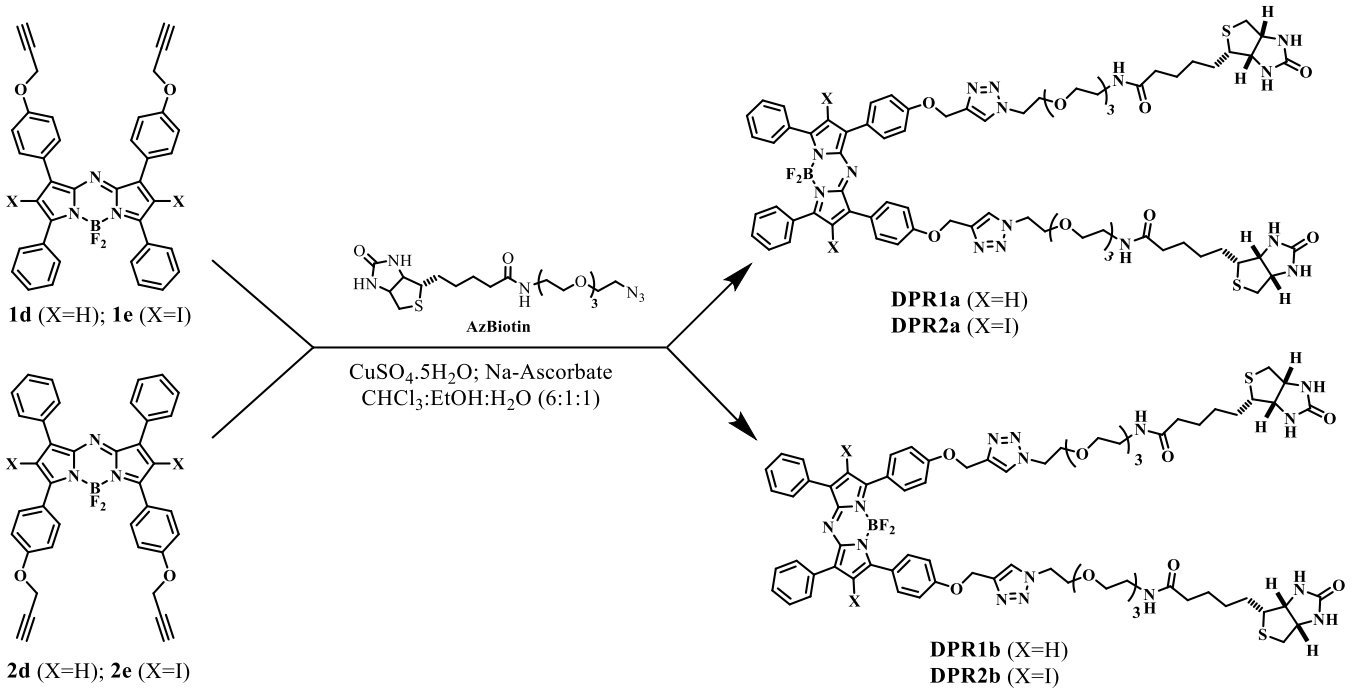

Table 1. Photophysical Properties of Aza-BODIPY-Biotin Conjugates

sensitizer	λ_{abs}, nm (ε, M^{-1} cm^{-1})	λ_{em}, nm[a]	fluorescence QY, Φ_F[ab]	triplet QY, Φ_T	singlet oxygen generation QY, $\Phi(^1O_2)$[c]
DPR1a	660 (106,500)	698	0.200	ND	ND
DPR1b	684 (80,000)	721	0.300	ND	ND
DPR2a	648 (67,000)	703	0.027	0.75	0.72
DPR2b	670 (63,500)	706	0.065	0.79	0.75
[d]**photofrin**	628 (3000)	630	0.10	0.61	0.30
[d]**Aza-BODIPY-5a**	660 (83,000)	706		0.68	0.65

[a]Excited at 620 nm. [b]Standard reference for fluorescence QY = 0.34 (ref 43). [c]Methylene blue was used as a standard for the singlet oxygen quantum yield standard, $\Phi(^1O_2)$ = 0.53; all the experiments were performed in methanol as a solvent; QY−quantum yield. [d]Literature data (refs 42 and 33); ND = not determined.

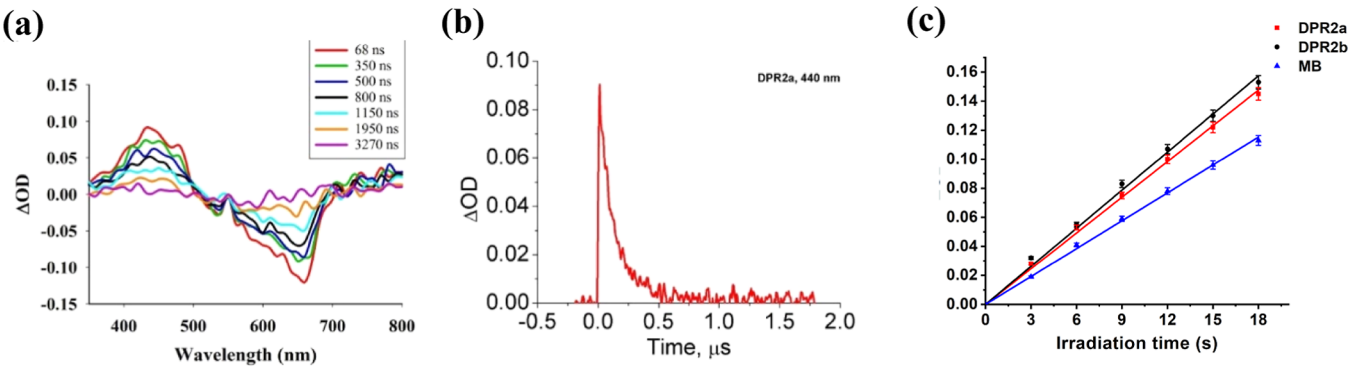

Figure 1. Transient absorption spectra of (a) **DPR2a** and (b) decay of the transient at 440 nm, excited by 355 nm laser pulse; time-resolved absorptions were recorded at 68, 350, 500, 800, 1150, 1950, and 3270 ns in methanol. (c) Graph of ΔOD of DPBF at 408 nm vs irradiation time for **DPR2a** and **DPR2b** against methylene blue (MB) as the standard in MeOH.

1d and **2d** with the azide-functionalized biotin-PEG_3 AzBiotin (Schemes 2 and 3). Regarding the synthesis of **DPR2a** and **DPR2b**, initially we attempted to iodinate both the aza-BODIPY conjugates **DPR1a** and **DPR1b** using NIS; however, we were unsuccessful. Alternatively, we tried to iodinate compounds **1d** and **2d**, which gave the iodinated compounds **1e** and **2e** (Scheme 1). Finally, both the iodinated compounds **1e** and **2e** were subjected to click reactions with AzBiotin to attain our desired aza-BODIPY-biotin conjugates **DPR2a** and **DPR2b**.

The conjugates **DPR1a**, **DPR1b**, **DPR2a**, and **DPR2b** showed good absorption in the therapeutic window at 660 nm (ϵ = 1.065 × 10^5 M^{-1} cm^{-1}), 684 nm (ϵ = 8.0 × 10^4 M^{-1} cm^{-1}), 648 nm (ϵ = 6.7 × 10^4 M^{-1} cm^{-1}), and 670 nm (ϵ =

https://doi.org/10.1021/acsomega.3c02416
ACS Omega 2023, 8, 26180−26190

Table 2. Comparative IC_{50} Values of DPR2a and DPR2b in Cancerous and Normal Cell Lines[a]

sensitizer	MDA-MB-231 breast cancer (μM)	MCF7 breast cancer (μM)	MiaPaCa pancreas cancer (μM)	SiHa cervical cancer (μM)	HEPG2 liver cancer (μM)	HT29 colon cancer (μM)	HSC4 oral cancer (μM)	MCF10A normal cell line (μM)
DPR2a	3	5	10	7.5	12	13	15	30
DPR2b	6	7	9	8.5	8.9	10.5	12	35
Photofrin	12							

[a]The analyses were carried out in triplicates, and data is shown as a standard deviation from the mean $n = 3$.

6.35×10^4 M^{-1} cm^{-1}), respectively, compared to Photofrin 628 nm (ϵ = 3000 M^{-1} cm^{-1}).[42] The emission spectra of **DPR1a**, **DPR1b**, **DPR2a**, and **DPR2b** exhibited emission in the range of 640−850 nm with the maxima at 698, 721, 703, and 706 nm, respectively, with fluorescence quantum yields (Φ_F) of 0.20, 0.30, 0.027, and 0.065, respectively, in methanol (Table 1).

We conducted nanosecond laser flash photolysis experiments[33] with **DPR2a** and **DPR2b** in MeOH to better understand the transitory intermediates of these systems (Figure 1 and details are given in the Supporting Information). We evaluated the transient absorptions of **DPR2a** and **DPR2b** in MeOH after illumination with 355 nm laser pulses (10 ns, 50 mJ/pulse), which resulted in transient absorptions at 440 and 380 nm, respectively. Within the laser pulse, transient absorptions of **DPR2a** at 440 nm and **DPR2b** at 380 nm decay by a first-order process with lifetimes of 0.5 and 0.6 s, respectively (Figure 1a,b and details are given in the Supporting Information).

Furthermore, the triplet-state quantum yields of our aza-BODIPYs were evaluated by a triplet−triplet energy-transfer method with β-carotene as the acceptor and tris(bipyridyl)-ruthenium(II) complex as the standard.[33] We measured the triplet quantum yield for **DPR2a** and **DPR2b** and found Φ_T = 0.75 ± 0.02 and 0.79 ± 0.02, respectively, which were better than those of Photofrin[42] and aza-BODIPY-5a[33] (Table1).

We also examined the singlet oxygen generation efficacy of **DPR2a** and **DPR2b** using the chemical trapping method using a singlet oxygen scavenger, 1,3-diphenylisobenzofuran (DPBF), to get an insight into their PDT efficacy. A solution of **DPR2a** and **DPR2b** with DPBF was irradiated by a 200W xenon lamp (620 nm), and variation in DPBF absorption was recorded with time (Figure 1c and details are given in the Supporting Information). The singlet oxygen generation efficiency (Φ^1O_2) of **DPR2a** and **DPR2b** was measured and found to be 0.72 ± 0.02 and 0.75 ± 0.02, respectively. Intriguingly, **DPR2a** and **DPR2b** showed superior photophysical properties over **aza-BODIPY-5a** and Photofrin[33,42] (Table 1).

2.2. Evaluation of In Vitro Photodynamic Therapy. With excellent photophysical results, we explored the photobiological aspects of aza-BODIPYs **DPR2a** and **DPR2b**. We first performed photocytotoxicity studies in various cancer cell lines such as MDA-MB-231, MCF7 breast cancer, HSC4 oral cancer, HEPG2 liver cancer, SiHa cervical cancer, MiaPaCa pancreas cancer, and HT29 colon cancer using the standard colorimetric (MTT) assay. Cytotoxic analyses have shown that aza-BODIPYs are non-cytotoxic under dark and light controls. Both the PSs **DPR2a** and **DPR2b** were examined in these cell lines under alike conditions with and without irradiation, and the growth inhibition percentages are depicted in Table 2. It was evident to find out that among all the cancer cells, MDA-MB-231 cells exhibited low IC_{50} values of 3 and 6 μM for **DPR2a** and **DPR2b**, respectively.[20] These results suggest that our PSs exhibit significant photocytotoxicity when activated by light even though they are neither cytotoxic nor toxic in the dark as compared to Photofrin (Figure 2 and details are given in the Supporting Information). However, some reports of small aza-BODIPYs are there with even better results.[9,43]

To comprehend the cellular uptake and distribution of **DPR2a** and **DPR2b**, confocal microscopy images were acquired in the MDA-MB-231 human breast cancer cell line using DAPI at different intervals (Figure 3a,b). It was fascinating to discover that within 15 and 30 min of incubation, both the PSs **DPR2a** (10 μM) and **DPR2b** (10 μM) were rapidly distributed in the MDA-MB-231 breast cancer cells. Strong and punctate luminescence surrounding the nucleus was found in combined images of MDA-MB-231 stained with PSs and DAPI, suggesting cytoplasmic affinity. These interesting results reflect the rapid cellular intake of our PSs in the cytosol of the cancer cells.

Furthermore, we also investigated the fluorescence images of **DPR2a** and **DPR2b** in biotin-negative non-cancerous MCF10A cell lines. Interestingly, in MCF10A cell lines, the PSs hardly showed any fluorescence upon excitation (Figure 3c). These results clearly show how **DPR2a** and **DPR2b** can selectively distinguish non-cancerous cells and cancerous cells.

In general, PDT has been linked to cell death caused by ROS. So, the CM-H_2DCFDA assay was used to study the cellular oxidative stress in **DPR2a**- and **DPR2b**-based PDT.[44] At concentrations of 1.5 and 3.5 μM of **DPR2a** and **DPR2b**, we observed DCFDA fluorescence of 80.4 and 89.9% in cells, respectively. After increasing the concentration to 3 and 6 μM compound **DPR2a** and **DPR2b**, respectively, the cells showed about 82.5 and 92.6% of DCFDA fluorescence, respectively (Figure 4a). On the other hand, hardly any fluorescence was detected under light and dark controls. This finding clearly shows that PDT with **DPR2a** and **DPR2b** significantly increased subcellular ROS production, which resulted in cellular damage in MDA-MB-231 cells.

The mitochondrial membrane potential by our PSs was further investigated by the TMRM staining experiment.[44] PDT treatment of MDA-MB-231 cells with **DPR2a** and **DPR2b** at 3 and 6 μM concentrations resulted in 40.3 and 41.6% reduction in membrane potential, respectively. However, in the light and dark controls, the mitochondrial membrane potential was only reduced to 7 and 9%, respectively. These findings demonstrate that **DPR2a** and **DPR2b** trigger cell death primarily *via* the apoptotic route during PDT treatment (Figure 4b and details are given in the Supporting Information).

Moreover, the membrane damage was validated using chromatin condensation fluorescence imaging with Hoechst.[44] After PDT treatment with **DPR2a** and **DPR2b** at 1.5−3 and 3−6 μM doses, chromatin condensation was detected in MDA-MB-231 cells. However, there was no chromatin condensation for the light or dark control, indicating a

https://doi.org/10.1021/acsomega.3c02416
ACS Omega 2023, 8, 26180−26190

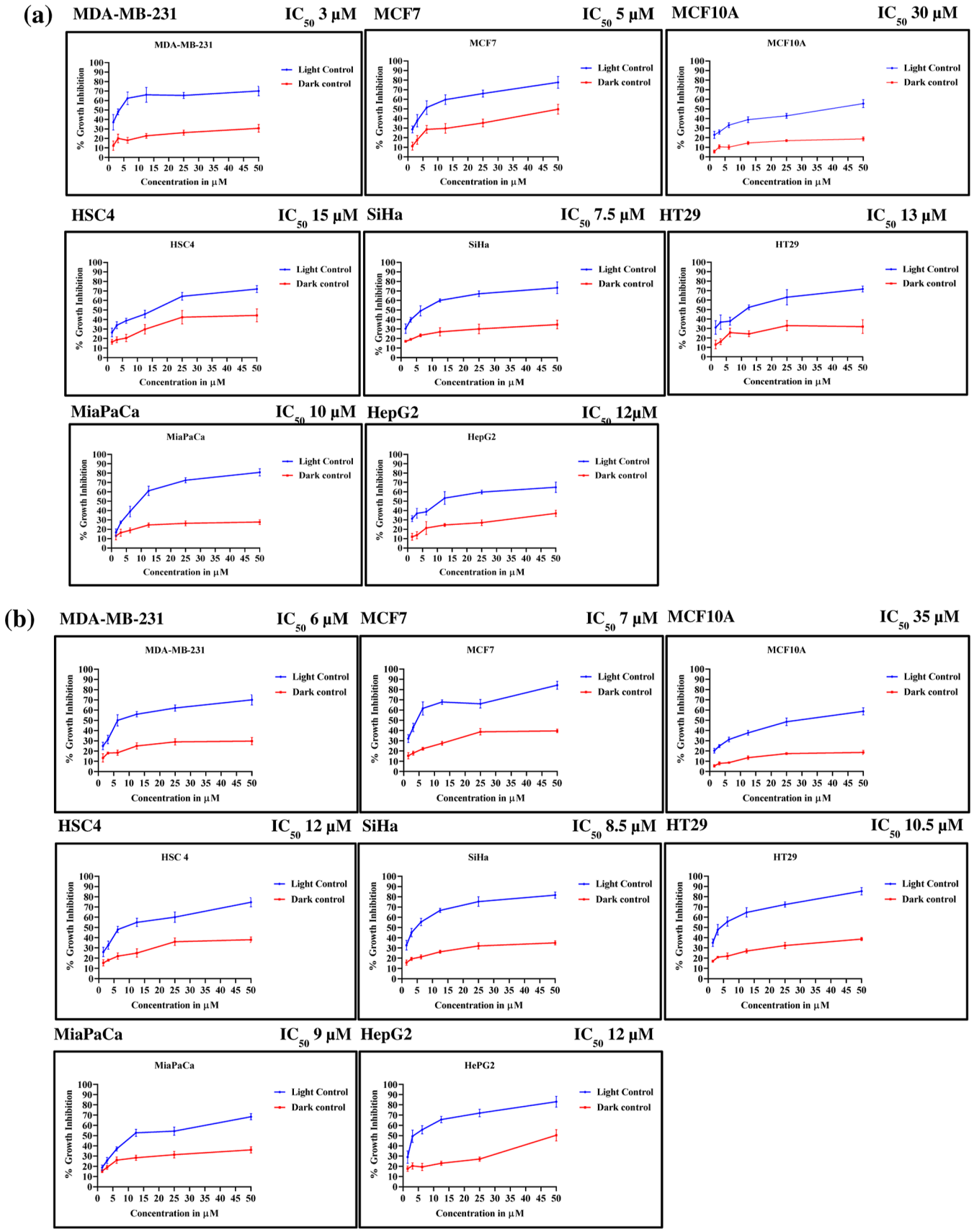

Figure 2. Photocytotoxicity of aza-BODIPY-biotin conjugates (a) **DPR2a** and (b) **DPR2b** in the presence and absence of light in various cancerous cell lines.

https://doi.org/10.1021/acsomega.3c02416
ACS Omega 2023, 8, 26180−26190

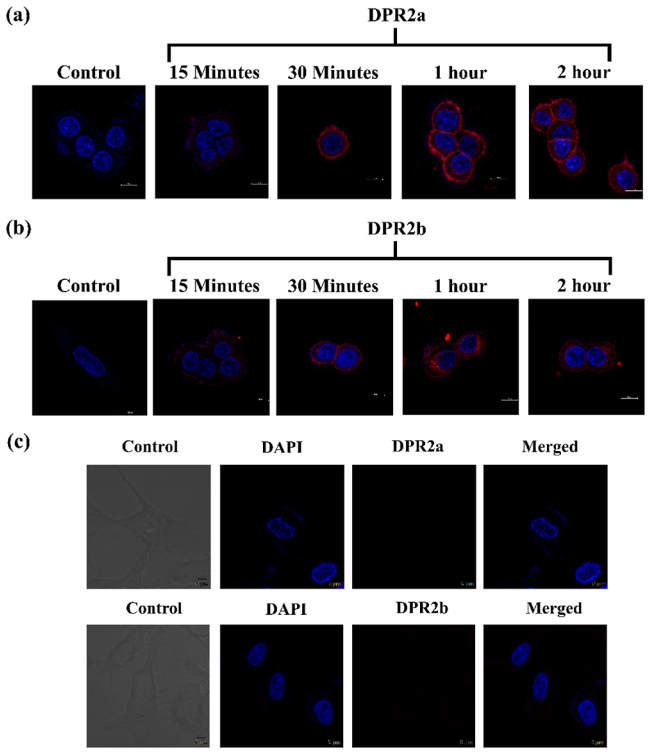

Figure 3. Cellular uptake studies of (a) **DPR2a**; (b) **DPR2b** by the MDA-MB-231 breast cancer cell line, scale bar: control—10 μm (DPR2a), 20 μm (DPR2b), and DPR2a or DPR2b—10 μm; and (c) **DPR2a** and **DPR2b** in the MCF10A non-cancerous cell line, scale bar—5 μm. Blue is the DAPI stain showing MDA-MB-231 or MCF10A cell nuclei and in red the aza-BODIPY-biotin conjugates **DPR2a** and **DPR2b** in the cytoplasm.

progressive elimination of malignant cells based on concentration due to the PDT actions of aza-BODIPY-biotin conjugates **DPR2a** and **DPR2b**.

Different phases in the cell cycle pattern serve as quality control measures for DNA and chromosome replication. Under this investigation, the cells were photo-treated with **DPR2a** and **DPR2b**, and their effect on cell cycle was observed. Interestingly, 26 and 20.6% of the G2/M arrest were found post PDT treatment as shown in Figure S6 in the Supporting Information. These results further establish that the cellular damage from our PSs is unrepairable and thus leads to apoptosis.

Further, Annexin V-FITC/PI assay was employed to elucidate the mechanism underlying the PDT activity and oxidative stress triggered by **DPR2a** and **DPR2b**[44] (Figure 4c). In this study, most of the cells did not show any apoptotic or necrotic changes when treated with **DPR2a** (3 μM) and **DPR2b** (6 μM) in the dark, indicating non-toxicity to MDA-MB-231 cells in the dark. Interestingly, after irradiation, the quantity of cells at the bottom right quadrant (Q4), which signifies the early apoptotic phase, and the top right quadrant (Q2), which signifies the late apoptotic phase, increases from 18 to 39.7% and 4.1 to 57.4%, respectively, when the concentration of **DPR2a** increases from 1.5 to 3 μM. Similarly, the percentage of cells at Q4 and Q2 increased from 20.7 to 41.3% and 7.7 to 51.8%, respectively, when the concentration of **DPR2b** increases from 3 to 6 μM. These findings reveal the apoptosis cancer cell death mechanism induced by our conjugates **DPR2a** and **DPR2b**.

2.3. Demonstration of the In Vivo PDT Activity. The exceptional in vitro photodynamic cytotoxicity of **DPR2a** against MDA-MB-231 breast cancer cells in vitro motivated us to investigate the in vivo PDT efficiency on a female NOD SCID animal. MDA-MB-231 cells (3−5 × 10^6 cells, 200 μL) were administered intravenously into the posterior flanks of the animal and left for one to two weeks for inducing tumor growth. The animals were then separated into two groups after being injected with cancer cells. The first group of six tumor-bearing mice served as controls (untreated), while the second group was exposed to PDT with **DPR2a**. The PS, **DPR2a** (in physiological saline), was injected intravenously into anesthetized mice, which were subsequently subjected to light (630 nm, 700 mW/cm^2) for 5 min.[42] Figure 5 shows the results of a 5 week observation of tumor volumes (TV, mm^3). When tumor volumes exceeded 10% of body weight, animals were slaughtered in accordance with ethical animal guidelines.

Figure 5a,b depicts the tumor volumes measured on the 1st day (before **DPR2a** treatment) and the 33rd day. After 33 days, the tumor volumes in irradiation-exposed animal models treated with **DPR2a** were no longer quantifiable. The experiments validate that the untreated mice exhibited massive tumor growth, while the **DPR2a** PDT-treated mice demonstrated an effective reduction in tumor volumes below quantifiable dimensions, in as little as 33 days, with no discernible scar at the tumor site (Figure 5c,d). The inhibition in the growth of breast tumor in mice model by **DPR2a** clearly signifies its potential for PDT application.

3. CONCLUSIONS

In summary, the synthesized aza-BODIPY-biotin conjugates **DPR2a** and **DPR2b** showed a favorable absorption range (600−750 nm), with excellent triplet excited-state quantum yields (up to 79%) and singlet oxygen generation efficiency (up to 75%). The in vitro PDT investigations of **DPR2a** and **DPR2b** in MDA-MB-231 breast cancer cells exhibited good fluorescence imaging with rapid localization in the cytoplasm within 15 min of incubation, with photocytotoxicity of 3 and 6 μM, respectively. Annexin V, TMRM, nuclear condensation, and DCFDA assay revealed cellular death to occur *via* the apoptosis pathway predominantly involving ROS intermediates. We also observed efficient inhibition of tumor growth in NOD/SCID mice with **DPR2a** PDT. Our results demonstrate that both the PSs **DPR2a** and **DPR2b** are promising candidates for imaging and PDT of cancer.

4. EXPERIMENTAL SECTION

4.1. Photophysical Studies. *4.1.1. Spectral Properties.* Absorption spectra were recorded in a HITACHI (U-3900) UV−vis spectrophotometer, and emission spectra were monitored in a Horiba (Fluorolog-3) fluorescence spectrophotometer. An applied Photophysics (LKS-20) laser kinetic spectrophotometer equipped with a Quanta Ray OCR-12 Series Nd/YAG nanosecond laser was used for the triplet excited-state study.[44]

4.1.2. Quantification of Fluorescence Quantum Yield. The fluorescence quantum yields (Φ_F) of our aza-BODIPY-biotin conjugates were measured employing aza-BODIPY **18b** as a standard (Φ_F = 0.36 in $CHCl_3$) reported by O'Shea et al.[43] The emission spectra of **DPR1a**, **DPR1b**, **DPR2a**, and **DPR2b** were monitored from 640 to 900 nm on excitation at 620 nm. The absorbance (optical density, OD) of all the aza-BODIPY-

https://doi.org/10.1021/acsomega.3c02416
ACS Omega 2023, 8, 26180−26190

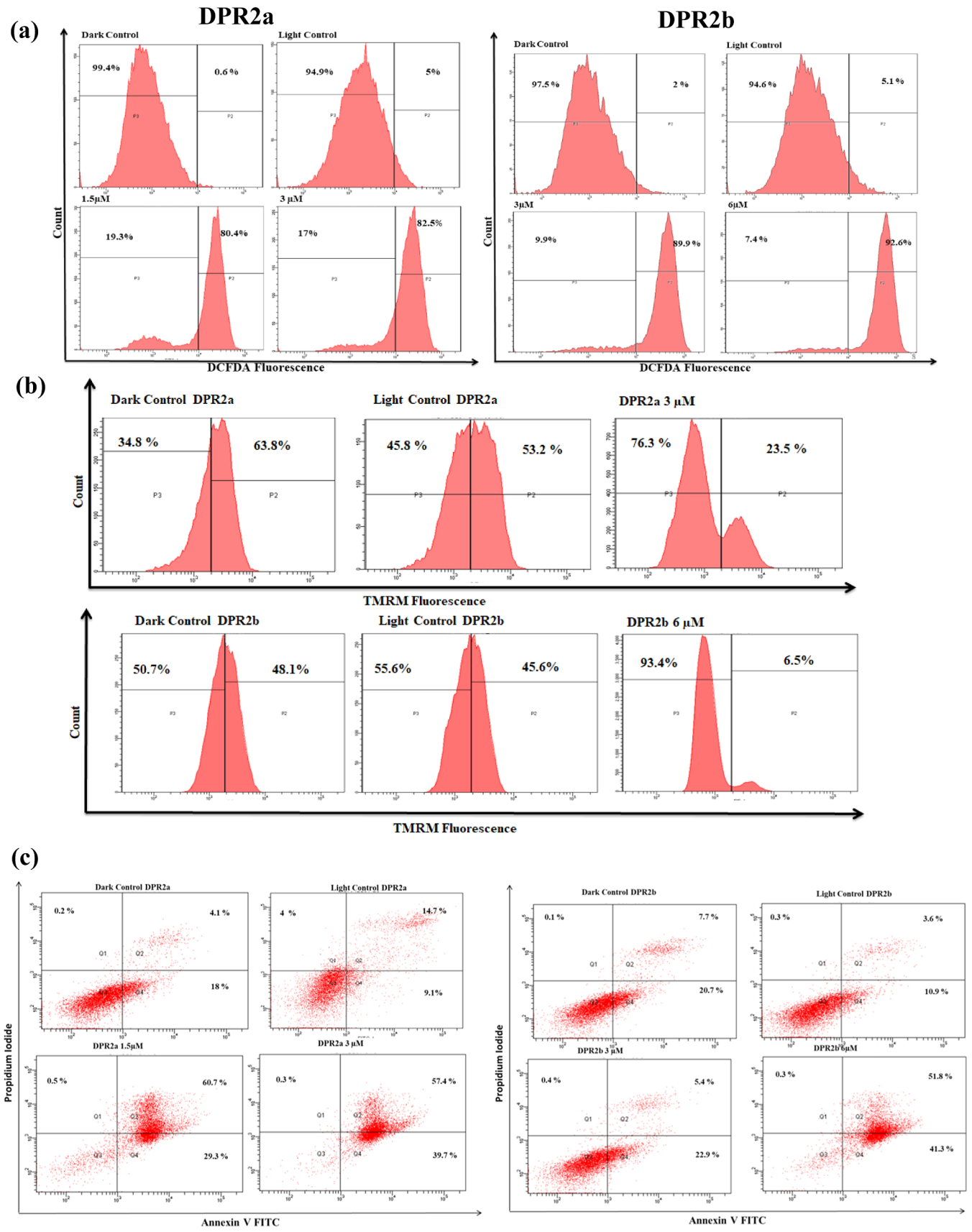

Figure 4. (a) ROS detection using DCFDA fluorescence under dark control, light control, after PDT with aza-BODIPY **DPR2a** and **DPR2b**; (b) TMRM assay flow cytometric evaluation of MDA-MB-231 cells, displaying reduction in $\Delta\psi$M by **DPR2a** and **DPR2b** PDT under light and dark controls; and (c) flow cytometric evaluation of MDA-MB-231 cells post PDT by **DPR2a** (1.5 and 3 μM) and **DPR2b** (3 and 6 μM).

https://doi.org/10.1021/acsomega.3c02416
ACS Omega 2023, 8, 26180−26190

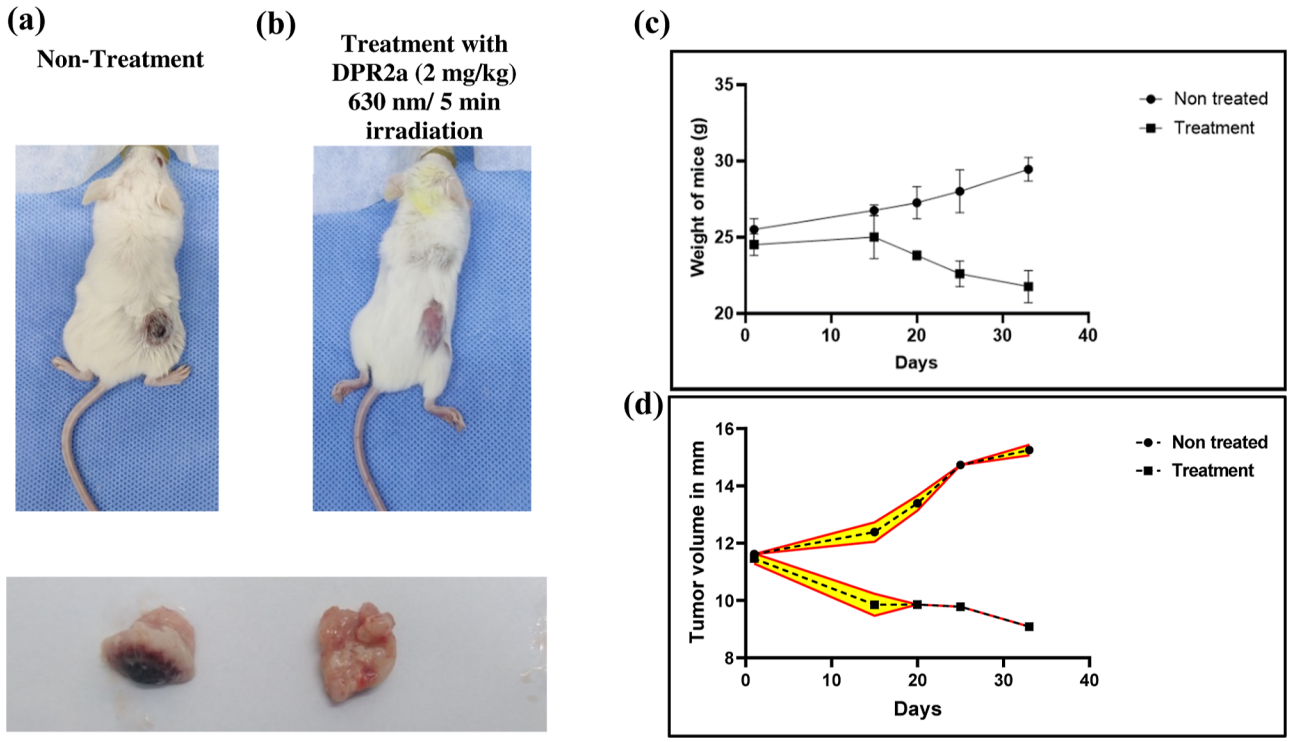

Figure 5. PDT against MDA-MB-231 cancer cells using **DPR2a** (2 mg/Kg body weight) in NOD/SCID mice. Representative gross images of mice bearing subcutaneous tumors (a) without drug (untreated) and (b) by irradiating in the presence of **DPR2a** after 33 days of incubation. Graph of change in (c) weight of mice (in g) and (d) tumor volume (in mm) vs days of treatment. The mean tumor volumes in different treatment groups were measured in every alternative day of drug treatment. Light irradiation: 630 nm, 700 mW/cm^2 for 5 min.

biotin conjugates was recorded at 620 nm, and Φ_F were evaluated according to eq 1

$$\Phi_{sample} = \Phi_{std} \times \left(\frac{A_{sample}}{A_{std}}\right) \times \left(\frac{OD_{std}}{OD_{sample}}\right) \times \left(\frac{n_{std}}{n_{sample}}\right)^2 \quad (1)$$

where Φ_{sample} and Φ_{std} are the quantum yields of the aza-BODIPY-biotin conjugate and the standard. A_{sample} and A_{std} are the areas under the emission spectra of the aza-BODIPY-biotin conjugate and the standard. OD_{sample} and OD_{std} are the absorbances of the aza-BODIPY-biotin conjugate and the standard measured at the excitation wavelength. n_{sample} and n_{std} are the refractive indices of the solvents of the aza-BODIPY-biotin conjugate and the standard.

4.1.3. Quantification of Triplet Excited States. We monitored the transient absorption spectra of aza-BODIPY-biotin conjugates **DPR2a** and **DPR2b** (in methanol) after exciting with a 355 nm laser pulse (85 mJ).

Transient-state quantum yields were measured using our previously used method of triplet−triplet energy transfer to β-carotene with Ru $(bpy)_3^{2+}$ as a standard.[45] A solution of β-carotene (THF) was added to an optically comparable solution of aza-BODIPY-biotin conjugates and standard Ru $(bpy)_3^{2+}$ and excited with a 355 nm laser pulse. The triplet transient absorbance (ΔA) of β-carotene at 510 nm due to the energy transfer from the standard and the aza-BODIPY-biotin conjugates was monitored. Through a correlation of the absorbance peaks after the complete triplet production, we estimated the triplet-state quantum yield (Φ_T) of **DPR2a** (Φ_T = 0.75 ± 0.02) and **DPR2b** (Φ_T = 0.79 ± 0.02) by using eq 2

$$\Phi_T^{abod} = \Phi_T^{std} \frac{\Delta A^{abod}}{\Delta A^{std}} \frac{k_{obs}^{abod}}{k_{obs}^{abod} - k_0^{abod}} \frac{k_{obs}^{std} - k_0^{std}}{k_{obs}^{std}} \quad (2)$$

Here, "std" and "abod" refer to the standard $Ru(bpy)_3^{2+}$ and the aza-BODIPY-biotin conjugates, respectively, "k_{obs}" is the β-carotene triplet formation rate constant, and "k_o" is the rate constant for the decay of donor triplets of the standard or the aza-BODIPY-biotin conjugates in the absence of β-carotene.

4.1.4. Quantification of Singlet Oxygen Generation Efficiency. The singlet oxygen quantum yield was evaluated by our previously employed chemical trapping method using the singlet oxygen scavenger DPBF.[46] An Oriel optical bench (model 11200) with a light source of a 200 W mercury lamp with a grating monochromator (model 77250) and appropriate high pass/bandwidth filters were used for irradiation. The $\Phi(^1O_2)$ values were calculated by irradiating an optically comparable solution of the aza-BODIPY-biotin conjugates and the standard, and the photo-oxidation of DPBF was determined using eq 3. Methylene blue ($\Phi(^1O_2)$ = 0.53) was used as the standard for the calculation of singlet oxygen generation quantum yields of **DPR2a** ($\Phi(^1O_2)$ = 0.72 ± 0.02) and **DPR2b** ($\Phi(^1O_2)$ = 0.75 ± 0.02).

$$\Phi(^1O_2)^{abod} = \Phi(^1O_2)^{ref} \frac{m^{abod} F^{ref}}{m^{ref} F^{abod}} \quad (3)$$

wherein "m" is the slope for the changes in the absorbance of DPBF (408 nm) vs irradiation time plot, $F = 1-10^{-OD}$, the absorption correction factor, and "abod" and "std" stand for the aza-BODIPY-biotin conjugate and the standard, respectively.

4.2. In Vitro *Photodynamic Therapy*. *4.2.1. Cell Culture.* Human breast cell lines MDA-MB-231, MCF7, HT29, HepG2,

https://doi.org/10.1021/acsomega.3c02416
ACS Omega 2023, 8, 26180−26190

SiHa, MiaPaCa, and HSC4 were procured from American Type Culture Collection (ATCC) and maintained in Dulbecco's modified Eagle's medium (DMEM) containing 10% fetal bovine serum (FBS) (Gibco, USA) and 1% antibiotic antimycotic cocktail (Gibco, USA) at 37 °C in 5% CO_2. MCF10A cells were cultured in DMEM/Nutrient F12-Ham medium (Sigma, USA) supplemented with 10% FBS, 20 ng/mL epidermal growth factor, 100 ng/mL cholera toxin, 0.01 mg/m insulin transferrin selenium, 500 ng/mL hydrocortisone, and 1 ng/m fibroblast growth factor (Sigma, USA).

4.2.2. Cytotoxicity Assay. For assessing cell viability, the MTT assay [3-(4,5-dimethylthiazol-2-yl)-2,5-diphenyltetrazolium bromide] was done. Briefly, 1×10^4 cells (cell counting was done using a hemocytometer, Sigma) were seeded in a 96-well culture dish. Cells were given PDT treatment (1−100 μM) of **DPR2a** and **DPR2b** aza-BODIPY for 24 h, and MTT was added at a final concentration of 500 μg/mL. The crystals of formazans were dissolved in isopropanol after 4 h of MTT addition, and the optical density was measured at 570 nm.

4.2.3. Cellular Uptake Studies. For cellular uptake studies, breast cancer cell lines MDA-MB-231 and MCF7 and the immortalized normal cell line MCF10A were seeded in 96-well opti-bottom plates (24 h incubation) and then treated with **DPR2a** and **DPR2b** aza-BODIPY. The triplicate wells were incubated for 10, 15, 20, 30, 60, and 120 min, and cells were fixed using 4% paraformaldehyde. The confocal laser scanning microscopic images show the subcellular level distribution of the PS. An excitation/emission at 588/610 nm has been used for **DPR2a** and **DPR2b** aza-BODIPY, and cells were further stained with nuclear stain DAPI.

4.2.4. ROS Detection. In a 60 mm culture dish, 1×10^6 MDA-MB-231 cells were sown. After 24 h of exponential growth, the cells were treated with **DPR2a** and **DPR2b** aza-BODIPY (1.5−6 μM) for 1 h followed by PDT using the VINVISH laser system (630 nm, 700 mW for 15 min). ROS was measured by flow cytometry using the CM-H_2DCFDA dye after 1 h post PDT treatment.

4.2.5. Cell Cycle Analysis. 1×10^6 MDA-MB-231 cells were sown in a 60 mm culture plate, and after 24 h, IC_{50} concentrations of **DPR2a** and **DPR2b** aza-BODIPY were added. After that, PDT treatment for 15 min was executed. Cells exposed to laser alone were taken as a light control, and cells incubated with **DPR2a** and **DPR2b** aza-BODIPY without laser irradiation were taken as a dark control. After treatment, the cells were incubated for different time-dependent intervals (3, 6, 12, 16, and 24 h). After trypsinization, the cells were harvested by centrifugation at 1200*g* for 5 min at 4 °C. The fixed cells were further incubated with RNase A (100 mg/mL) for another 1 h at 37 °C and later for another 15 min with propidium iodide (10 mg/mL) in the dark. Finally, analysis was done using FACS Aria for DNA content.

4.2.6. TMRM Assay. In a 60 mm culture dish, 1×10^6 MDA-MB-231 cells were sown. After 24 h of exponential growth, the cells were treated with **DPR2a** (1.5−6 μM) and **DPR2b** (3−8 μM) aza-BODIPY for 1 h followed by PDT using the VINVISH laser system (630 nm, 700 mW for 15 min). The mitochondrial potential was measured by flow cytometry using the TMRM dye after 20 min post PDT.

4.2.7. Annexin Binding Assay. Briefly, 1×10^6 cells were initially counted and seeded in a 60 mm culture plate. Post 24 h of seeding, the cells were given PDT treatment as mentioned earlier for 24 h. The cells were rinsed with 1 × PBS before being trypsinized and pelleted by centrifugation at 400*g* for 3 min at 4 °C. For the staining, 3 μL of FITC-conjugated Annexin was appended to the cell suspension in a binding buffer (supplied in the kit Sigma-Aldrich USA) and incubated in the dark for 15 min at 37 °C. The cells were then rinsed with the binding buffer before carrying out flow cytometric analysis using FACS Aria.

4.3. In Vivo Photodynamic Therapy. To build xenograft tumors, MDA-MB-231 human breast cancer cells were administered to the female NOD/SCID mice in the dorsal flank. Once the tumors became palpable, their sizes were measured, and the mice were randomly divided into two groups such as group I non-treated control and group II aza-BODIPY **DPR2a** 2 mg/kg. Animals were injected I.P. with the given doses, and after 24 h, laser irradiation was done using the VINVISH PDT laser system coupled with an optical fiber (630 nm, 700 mW/cm^2 for 5 min). PDT treatment was conducted twice a week. Before PDT treatment was carried out, tumors were permitted to reach a size of 5−6 mm in diameter. Once visible tumor appeared, its volume was measured using callipers every 2 days for obtaining the rate of tumor growth in both groups. The tumor volume was calculated using the formula $V(\text{mm}^3) = (\text{largest length}) \times (\text{shortest length})^2$. At the end, mice were sacrificed using carbon dioxide inhalation and images were captured.

■ ASSOCIATED CONTENT

Supporting Information

The Supporting Information is available free of charge at https://pubs.acs.org/doi/10.1021/acsomega.3c02416.

General information; synthesis of starting materials, **DPR2a** and **DPR2b**; transient absorption of DPR2b; absorption spectra of DPBF after irradiation in the presence of PSs; photocytotoxicity of Photofrin; TMRM assay; chromatin condensation; cell cycle analysis; and ^{1}H, ^{13}C NMR, and HRMS spectra of all the synthesized compounds and HPLC chromatogram of **DPR2a** and **DPR2b** (PDF)

■ AUTHOR INFORMATION

Corresponding Authors

S. Asha Nair − *Cancer Research Program 4, Rajiv Gandhi Centre for Biotechnology, Trivandrum, Kerala 695014, India;* orcid.org/0000-0002-3756-3259; Email: sasha@rgcb.res.in

Pranjal Gogoi − *Applied Organic Chemistry Group, Chemical Science and Technology Division, CSIR-North East Institute of Science and Technology (CSIR-NEIST), Jorhat, Assam 785006, India; Academy of Scientific and Innovative Research (AcSIR), Ghaziabad 201002, India;* orcid.org/0000-0003-0711-0328; Email: gogoipranj@yahoo.co.uk, gogoipranj@gmail.com

Authors

Dhiraj Dutta − *Applied Organic Chemistry Group, Chemical Science and Technology Division, CSIR-North East Institute of Science and Technology (CSIR-NEIST), Jorhat, Assam 785006, India; Academy of Scientific and Innovative Research (AcSIR), Ghaziabad 201002, India;* orcid.org/0000-0002-4629-9808

Rajshree R. Nair − *Cancer Research Program 4, Rajiv Gandhi Centre for Biotechnology, Trivandrum, Kerala 695014,*

https://doi.org/10.1021/acsomega.3c02416
ACS Omega 2023, 8, 26180−26190

India; Manipal Academy of Higher Education, Manipal, Karnataka 576104, India

Sreejith Mangalath − *Photosciences and Photonics Section, Chemical Sciences and Technology Division, CSIR-National Institute for Interdisciplinary Science and Technology (CSIR-NIIST), Trivandrum 695019, India;* orcid.org/0000-0001-8914-0293

Joshy Joseph − *Academy of Scientific and Innovative Research (AcSIR), Ghaziabad 201002, India; Photosciences and Photonics Section, Chemical Sciences and Technology Division, CSIR-National Institute for Interdisciplinary Science and Technology (CSIR-NIIST), Trivandrum 695019, India;* orcid.org/0000-0002-4592-8991

Danaboyina Ramaiah − *Department of Chemistry, Birla Institute of Technology & Science (BITS), Hyderabad, Telangana 500078, India*

Complete contact information is available at: https://pubs.acs.org/10.1021/acsomega.3c02416

Author Contributions

¶D.D. and R.R.N. made equal contributions to this study.

Notes

The authors declare no competing financial interest.

All the experiments on NOD-SCID mice were performed after approval from the Institute Animal Ethics Committee (IAEC/798/ASN/2020).

■ ACKNOWLEDGMENTS

We are grateful to the Director, CSIR-NEIST, Jorhat, and RGCB, Trivandrum, India, for the interest in this work and facilities provided. The authors acknowledge the DBT (File no. BT/PR28133/NER/95/1383/2018), Government of India, for research funding. D.D. acknowledges the DST, New Delhi, India, for DST-Inspire fellowship grants (IF160502) funds, and R.R.N. acknowledges RGCB and ICMR SRF (Fellowship ID: 2021-11018-F1) fellowship for funding. D.R. thanks DST, New Delhi, India (SR/PURSE/2020/20), for the funding. We thank Jiji V, Ciji Varghese, and Soumya for confocal microscopic imaging and analysis. We thank Indu Ramachandran and Arya V S for flow cytometric analysis.

■ REFERENCES

(1) Correia, J. H.; Rodrigues, J. A.; Pimenta, S.; Dong, T.; Yang, Z. Photodynamic Therapy Review: Principles, Photosensitizers, Applications, and Future Directions. *Pharmaceutics* **2021**, *13*, 1332.

(2) Levy, J. G. Photosensitizers in Photodynamic Therapy. *Semin. Oncol.* **1994**, *21*, 4−10.

(3) Dougherty, T. J.; Gomer, C. J.; Henderson, B. W.; Jori, G.; Kessel, D.; Korbelik, M.; Moan, J.; Peng, Q. Photodynamic Therapy. *JNCI, J. Natl. Cancer Inst.* **1998**, *90*, 889−905.

(4) Dolmans, D. E. J. G. J.; Fukumura, D.; Jain, R. K. Photodynamic Therapy for Cancer. *Nat. Rev. Cancer* **2003**, *3*, 380−387.

(5) Zhao, X.; Liu, J.; Fan, J.; Chao, H.; Peng, X. Recent Progress in Photosensitizers for Overcoming the Challenges of Photodynamic Therapy: From Molecular Design to Application. *Chem. Soc. Rev.* **2021**, *50*, 4185−4219.

(6) Pham, T. C.; Nguyen, V. N.; Choi, Y.; Lee, S.; Yoon, J. Recent Strategies to Develop Innovative Photosensitizers for Enhanced Photodynamic Therapy. *Chem. Rev.* **2021**, *121*, 13454−13619.

(7) Lu, H.; MacK, J.; Yang, Y.; Shen, Z. Structural Modification Strategies for the Rational Design of Red/NIR Region BODIPYs. *Chem. Soc. Rev.* **2014**, *43*, 4778−4823.

(8) Gupta, I.; Kesavan, P. E. Carbazole Substituted BODIPYs. *Front. Chem.* **2019**, *7*, 841.

(9) Yu, Z.; Wang, H.; Chen, Z.; Dong, X.; Zhao, W.; Shi, Y.; Zhu, Q. Discovery of an Amino Acid-Modified Near-Infrared Aza-BODIPY Photosensitizer as an Immune Initiator for Potent Photodynamic Therapy in Melanoma. *J. Med. Chem.* **2022**, *65*, 3616−3631.

(10) Li, S.; Zou, Q.; Li, Y.; Yuan, C.; Xing, R.; Yan, X. Smart Peptide-Based Supramolecular Photodynamic Metallo-Nanodrugs Designed by Multicomponent Coordination Self-Assembly. *J. Am. Chem. Soc.* **2018**, *140*, 10794−10802.

(11) Liu, T. W. B.; Chen, J.; Zheng, G. Peptide-Based Molecular Beacons for Cancer Imaging and Therapy. *Amino Acids* **2011**, *41*, 1123−1134.

(12) Zhang, Q.; Cai, Y.; Li, Q. Y.; Hao, L. N.; Ma, Z.; Wang, X. J.; Yin, J. Targeted Delivery of a Mannose-Conjugated BODIPY Photosensitizer by Nanomicelles for Photodynamic Breast Cancer Therapy. *Chem.—Eur. J.* **2017**, *23*, 14307−14315.

(13) Cheng, M. H. Y.; Maruani, A.; Savoie, H.; Chudasama, V.; Boyle, R. W. Synthesis of a Novel HER2 Targeted Aza-BODIPY-Antibody Conjugate: Synthesis, Photophysical Characterisation and: In Vitro Evaluation. *Org. Biomol. Chem.* **2018**, *16*, 1144−1149.

(14) Nombona, N.; Maduray, K.; Antunes, E.; Karsten, A.; Nyokong, T. Synthesis of Phthalocyanine Conjugates with Gold Nanoparticles and Liposomes for Photodynamic Therapy. *J. Photochem. Photobiol., B* **2012**, *107*, 35−44.

(15) Li, D.; Wang, X. Z.; Yang, L. F.; Li, S. C.; Hu, Q. Y.; Li, X.; Zheng, B. Y.; Ke, M. R.; Huang, J. D. Size-Tunable Targeting-Triggered Nanophotosensitizers Based on Self-Assembly of a Phthalocyanine-Biotin Conjugate for Photodynamic Therapy. *ACS Appl. Mater. Interfaces* **2019**, *11*, 36435−36443.

(16) Han, Y.; An, Y.; Jia, G.; Wang, X.; He, C.; Ding, Y.; Tang, Q. Theranostic Micelles Based on Upconversion Nanoparticles for Dual-Modality Imaging and Photodynamic Therapy in Hepatocellular Carcinoma. *Nanoscale* **2018**, *10*, 6511−6523.

(17) Adarsh, N.; Babu, P. S. S.; Avirah, R. R.; Viji, M.; Nair, S. A.; Ramaiah, D. Aza-BODIPY Nanomicelles as Versatile Agents for the: In Vitro and in Vivo Singlet Oxygen-Triggered Apoptosis of Human Breast Cancer Cells. *J. Mater. Chem. B* **2019**, *7*, 2372−2377.

(18) Li, X.; Kim, C.; Lee, S.; Lee, D.; Chung, H.-M.; Kim, G.; Heo, S.-H.; Kim, C.; Hong, K.-S.; Yoon, J. Nanostructured Phthalocyanine Assemblies with Protein-Driven Switchable Photoactivities for Biophotonic Imaging and Therapy. *J. Am. Chem. Soc.* **2017**, *139*, 10880−10886.

(19) Chen, D.; Zhong, Z.; Ma, Q.; Shao, J.; Huang, W.; Dong, X.; Dong, X. Aza-BODIPY-Based Nanomedicines in Cancer Phototheranostics. *ACS Appl. Mater. Interfaces* **2020**, *12*, 26914−26925.

(20) Ren, W. X.; Han, J.; Uhm, S.; Jang, Y. J.; Kang, C.; Kim, J. H.; Kim, J. S. Recent Development of Biotin Conjugation in Biological Imaging, Sensing, and Target Delivery. *Chem. Commun.* **2015**, *51*, 10403−10418.

(21) Li, K.; Dong, W.; Liu, Q.; Lv, G.; Xie, M.; Sun, X.; Qiu, L.; Lin, J. A Biotin Receptor-Targeted Silicon(IV) Phthalocyanine for in Vivo Tumor Imaging and Photodynamic Therapy. *J. Photochem. Photobiol., B* **2019**, *190*, 1−7.

(22) Dong, W.; Li, K.; Wang, S.; Qiu, L.; Liu, Q.; Xie, M.; Lin, J. Targeted Photodynamic Therapy (PDT) of Lung Cancer with Biotinylated Silicon (IV) Phthalocyanine. *Curr. Pharm. Biotechnol.* **2021**, *22*, 414−422.

(23) Okoth, E. A.; Zhou, Z.; Ongarora, B.; Stutes, A.; Mathis, J. M.; Vicente, M. G. H. Synthesis and Investigation of Phthalocyanine-Biotin Conjugates. *J. Porphyr. Phthalocyanines* **2019**, *23*, 125−135.

(24) Purushothaman, B.; Choi, J.; Park, S.; Lee, J.; Samson, A. A. S.; Hong, S.; Song, J. M. Biotin-Conjugated PEGylated Porphyrin Self-Assembled Nanoparticles Co-Targeting Mitochondria and Lysosomes for Advanced Chemo-Photodynamic Combination Therapy. *J. Mater. Chem. B* **2019**, *7*, 65−79.

(25) Isaac-Lam, M. F.; Hammonds, D. M. Biotinylated Chlorin and Its Zinc and Indium Complexes: Synthesis and In Vitro Biological Evaluation for Photodynamic Therapy. *Pharmaceuticals* **2017**, *10*, 41.

(26) Isaac-Lam, M. F.; Mee, A. D. Photodynamic Activity of Vitamin-Chlorin Conjugates at Nanomolar Concentrations against

Triple-Negative Breast Cancer Cells. *ACS Omega* **2019**, *4*, 2907−2920.
(27) Li, M.; Xia, J.; Tian, R.; Wang, J.; Fan, J.; Du, J.; Long, S.; Song, X.; Foley, J. W.; Peng, X. Near-Infrared Light-Initiated Molecular Superoxide Radical Generator: Rejuvenating Photodynamic Therapy against Hypoxic Tumors. *J. Am. Chem. Soc.* **2018**, *140*, 14851−14859.
(28) Paul, S.; Kundu, P.; Bhattacharyya, U.; Garai, A.; Maji, R. C.; Kondaiah, P.; Chakravarty, A. R. Ruthenium(II) Conjugates of Boron-Dipyrromethene and Biotin for Targeted Photodynamic Therapy in Red Light. *Inorg. Chem.* **2020**, *59*, 913−924.
(29) Oliveira, G. D. F. S.; Gouveia, F. S.; Pinheiro, A. D. A.; do Nascimento Neto, L. G.; de Vasconcelos, M. A.; Teixeira, E. H.; Gondim, A. C. S.; Lopes, L. G. d. F.; de Carvalho, I. M. M.; Sousa, E. H. S.; Sousa, E. H. S. An Anthracene-Pendant Ruthenium(II) Complex Conjugated to a Biotin Anchor, an Essential Handle for Photo-Induced Anti-Cancer Activity. *New J. Chem.* **2020**, *44*, 6610−6622.
(30) Saha, S.; Majumdar, R.; Hussain, A.; Dighe, R. R.; Chakravarty, A. R. Biotin-Conjugated Tumour-Targeting Photocytotoxic Iron(III) Complexes. *Philos. Trans. R. Soc., A* **2013**, *371*, 20120190.
(31) Ge, Y.; O'Shea, D. F. Azadipyrromethenes: From Traditional Dye Chemistry to Leading Edge Applications. *Chem. Soc. Rev.* **2016**, *45*, 3846−3864.
(32) Shi, Z.; Han, X.; Hu, W.; Bai, H.; Peng, B.; Ji, L.; Fan, Q.; Li, L.; Huang, W. Bioapplications of small molecule Aza-BODIPY: from rational structural design to *in vivo* investigations. *Chem. Soc. Rev.* **2020**, *49*, 7533−7567.
(33) Adarsh, N.; Avirah, R. R.; Ramaiah, D. Tuning Photosensitized Singlet Oxygen Generation Efficiency of Novel Aza-BODIPY Dyes. *Org. Lett.* **2010**, *12*, 5720−5723.
(34) Yu, Z.; Zhou, J.; Ji, X.; Lin, G.; Xu, S.; Dong, X.; Zhao, W. Discovery of a Monoiodo Aza-BODIPY Near-Infrared Photosensitizer: In Vitro and in Vivo Evaluation for Photodynamic Therapy. *J. Med. Chem.* **2020**, *63*, 9950−9964.
(35) Murtagh, J.; Frimannsson, O.; O'Shea, D. F. Azide Conjugatable and PH Responsive Near-Infrared Fluorescent Imaging Probes. *Org. Lett.* **2009**, *11*, 5386−5389.
(36) Balsukuri, N.; Manav, N.; Lone, M. Y.; Mori, S.; Das, A.; Sen, P.; Gupta, I. Donor-Acceptor Architectures of Tetraphenylethene Linked Aza-BODIPYs: Synthesis, Crystal Structure, Energy Transfer and Computational Studies. *Dyes Pigm.* **2020**, *176*, 108249.
(37) Balsukuri, N.; Boruah, N. J.; Kesavan, P. E.; Gupta, I. Near Infra-Red Dyes Based on Pyrene Aza-BODIPYs. *New J. Chem.* **2018**, *42*, 5875−5888.
(38) Jiao, L.; Wu, Y.; Wang, S.; Hu, X.; Zhang, P.; Yu, C.; Cong, K.; Meng, Q.; Hao, E.; Vicente, M. G. H. Accessing Near-Infrared-Absorbing BF2-Azadipyrromethenes via a Push−Pull Effect. *J. Org. Chem.* **2014**, *79*, 1830−1835.
(39) Korpusik, A. B.; Tan, Y.; Garrison, J. B.; Tan, W.; Sumerlin, B. S. Aptamer-Conjugated Micelles for Targeted Photodynamic Therapy Via Photoinitiated Polymerization-Induced Self-Assembly. *Macromolecules* **2021**, *54*, 7354−7363.
(40) Treekoon, J.; Pewklang, T.; Chansaenpak, K.; Gorantla, J. N.; Pengthaisong, S.; Lai, R. Y.; Ketudat-Cairns, J. R.; Kamkaew, A. Glucose Conjugated Aza-BODIPY for Enhanced Photodynamic Cancer Therapy. *Org. Biomol. Chem.* **2021**, *19*, 5867−5875.
(41) Bandi, V.; El-Khouly, M. E.; Ohkubo, K.; Nesterov, V. N.; Zandler, M. E.; Fukuzumi, S.; D'Souza, F. Excitation-Wavelength-Dependent, Ultrafast Photoinduced Electron Transfer in Bisferrocene/BF2-Chelated-Azadipyrromethene/Fullerene Tetrads. *Chem.—Eur. J.* **2013**, *19*, 7221−7230.
(42) Marydasan, B.; Madhuri, B.; Cherukommu, S.; Jose, J.; Viji, M.; Karunakaran, S. C.; Chandrashekar, T. K.; Rao, K. S.; Rao, C. M.; Ramaiah, D. In Vitro and In Vivo Demonstration of Human-Ovarian-Cancer Necrosis through a Water-Soluble and Near-Infrared-Absorbing Chlorin. *J. Med. Chem.* **2018**, *61*, 5009−5019.
(43) Gorman, A.; Killoran, J.; O'Shea, C.; Kenna, T.; Gallagher, W. M.; O'Shea, D. F. In Vitro Demonstration of the Heavy-Atom Effect for Photodynamic Therapy. *J. Am. Chem. Soc.* **2004**, *126*, 10619−10631.
(44) Marydasan, B.; Nair, R. R.; Babu, P. S. S.; Ramaiah, D.; Nair, S. A.; Ramaiah, D.; Asha Nair, S. Picolyl Porphyrin Nanostructures as a Functional Drug Entrant for Photodynamic Therapy in Human Breast Cancers. *ACS Omega* **2019**, *4*, 12808−12816.
(45) Kumar, C. v.; Qin, L.; Das, P. K. Aromatic Thioketone Triplets and Their Quenching Behaviour towards Oxygen and Di-t-Butylnitroxy Radical. A Laser-Flash-Photolysis Study. *J. Chem. Soc., Faraday Trans. 2* **1984**, *80*, 783−793.
(46) Ramaiah, D.; Joy, A.; Chandrasekhar, N.; Eldho, N. v.; Das, S.; George, M. v. Halogenated Squaraine Dyes as Potential Photochemotherapeutic Agents. Synthesis and Study of Photophysical Properties and Quantum Efficiencies of Singlet Oxygen Generation. *Photochem. Photobiol.* **1997**, *65*, 783−790.

https://doi.org/10.1021/acsomega.3c02416
ACS Omega 2023, 8, 26180−26190